Supplemental Material: The structure and intermolecular forces of DNA condensates

Jejoong Yoo and Aleksei Aksimentiev*

Center for the Physics of Living Cells, Department of Physics,

University of Illinois at Urbana–Champaign,

1110 West Green Street, Urbana, Illinois 61801

(Dated: October 15, 2015)

* aksiment@illinois.edu

I. EVIDENCE OF SAMPLING AND REPRODUCIBILITY

To demonstrated adequate sampling of the microscopic configurations and reproducibility of our DNA array data, we performed a replicate simulation of the DNA array system at sub-mM Sm^{4+} concentration starting from the following extreme initial conditions: all Sm^{4+} molecules were placed outside the DNA array, Fig. S1 A.

A. Reproducibility of Sm^{4+} distributions

During the 190 ns simulation, Sm^{4+} molecules diffused into the DNA array, dispersing among the DNA helices in the same manner as in our previous simulation (compare Fig. S1 B and Fig. S1 C). Within the array, the distribution of Sm^{4+} matched the distribution observed in our previous simulation: four Sm^{4+} molecules were adsorbed to each DNA duplex; the remaining Sm^{4+} molecules could diffuse between the helices, Fig. S1 D–F. In our simulations, adsorption of Sm^{4+} molecules to DNA does not cause a sampling problem because the molecules bind to DNA reproducibly and stably. Diffusion of the remaining Sm^{4+} molecules is fast enough to sample the DNA array volume within 100 ns. For example, the average residence time of Sm^{4+} near a DNA phosphate is, at most, 5 ns Fig. S1 G. In 100 ns, the mean square displacement (MSD) of a Sm^{4+} molecule that is not bound to DNA is $\sim$80 nm^2 in a DNA array of $R = 12$ nm radius. The MSD drops by less than 15% at R =10 and 11 nm. Thus, Sm^{4+} molecules can diffuse across the entire DNA array within the timescale of our simulations.

B. Reproducibility of DNA pressure

To demonstrate reproducibility of the dependence of the DNA array's internal pressure on the average DNA–DNA distance, we carried out two additional simulations of the sub-mM [Sm^{4+}] DNA array system starting from the microscopic conformations obtained during the replicate DNA array simulation. In the first simulations, the radius of the DNA array was changed from 12 to 11 nm using a microscopic state observed after 120 ns from the beginning of the replicate simulation. The second simulation began using a microscopic state observed after 50 ns from the beginning of the first simulation; the radius of the DNA array was changed from 11 to 10 nm. Fig. S1 H illustrates the simulated dependences of the

DNA array pressure on the simulation time. The average pressure values obtained from the three (R =12, 11 and 10 nm) replicate simulations are in good agreement with our original data, Fig. 1D(iii). Because the sub-mM [Sm^{4+}] DNA array system is the most challenging among the systems investigated in our work with regard to convergence and reproducibility, all other systems can be safely assumed to be convergent.

C. Sampling of DNA conformations

For DNA array systems of internal pressure below ∼20 bar, the translational and rotational diffusion coefficients of DNA are ∼50 $nm^2/\mu s$ and ∼20 $rad^2/\mu s$, respectively, Fig. 3G. Thus, the mean translational and rotational displacements of DNA within 100 ns are ∼3 nm and ∼110°, respectively. Thus, DNA molecules, on average, can travel by diffusion the distance exceeding the average surface-to-surface distance between neighboring DNA molecules in a DNA array and can explore a wide range of mutual orientations. Another indication of convergence is the symmetric shape (with respect to $\Delta\theta = 180°$) of the probability distributions shown in Figs. 3C and 3D. When DNA pressure is extremely high (>50 bar), the sampling problem might occur. However, comparison of the results of our replicate and production simulations, main text Fig. 1D(iii), indicates that even at ∼50 bar, sampling does not present a problem for determining the average pressure or inter-DNA distance.

II. SM METHODS

A. Additional general MD methods

All MD simulations were carried out in a constant-temperature/constant-area ensemble using the Gromacs 4.5.5 package [1] and a 2 fs integration time step. The temperature was controlled using the Nosé-Hoover scheme [2, 3]. Temperature was set to 300 K in all simulations. The pressure was kept constant at 1 bar using the Parrinello-Rahman scheme [4]. A 7-to-8 Å switching scheme was applied to evaluate van der Waals forces. The long-range electrostatic forces were evaluated using the particle-Mesh Ewald (PME) summation scheme [5] over a 1.2-Å resolution grid and a 12 Å cutoff for the real-space Coulomb interaction. Covalent bonds to hydrogen in water and other molecules were kept rigid using the SETTLE [6] and LINCS [7] algorithms, respectively.

B. Calculations of the interaction-type dependent contributions to the PMFs

We note that the following derivation in this section is adopted from the literature [8–11]. We summarize the derivations here to clarify the formula we used.

We consider a system of N atoms. The coordinate and mass of atom j are $\vec{r}_j = (x_j, y_j, z_j)$ and m_j, respectively. We define reaction coordinate ξ for the two-helix system as the distance between the centers of mass of the helices, R_1 and R_2, projected onto the xy plane:

$$\xi = |\vec{R}_1 - \vec{R}_2|, \tag{1}$$

where

$$\vec{R}_i = (X_i, Y_i) = \left(\frac{\sum_j^{\mathrm{DNA}_i} m_j x_j}{\sum_j^{\mathrm{DNA}_i} m_j}, \frac{\sum_j^{\mathrm{DNA}_i} m_j y_j}{\sum_j^{\mathrm{DNA}_i} m_j} \right). \tag{2}$$

Hereafter, we denote a sum over all atoms of each helix using $\sum_j^{\mathrm{DNA}_1} \cdots$ and $\sum_j^{\mathrm{DNA}_2} \cdots$ notations. Instantaneous force along the reaction coordinate ξ, F_ξ, is

$$F_\xi(\xi) = -\frac{\partial U(\vec{\mathbf{r}})}{\partial \xi} = \sum_{j=1}^{N} \vec{F}_j \cdot \frac{\partial \vec{r}_j}{\partial \xi} = \left(\sum_j^{\mathrm{DNA}_1} \vec{F}_j - \sum_j^{\mathrm{DNA}_2} \vec{F}_j \right) \cdot \frac{\vec{R}_1 - \vec{R}_2}{2\xi} \tag{3}$$

where $U(\vec{\mathbf{r}})$ is the potential energy and $\vec{F}_j = -\nabla_j U(\vec{\mathbf{r}})$ is the force on atom j [8–11]. For

the third equality in Eq. (3), we used the following relationship:

$$\frac{\partial \vec{r}_j}{\partial \xi} = \left\{ \begin{array}{ll} \frac{\vec{R}_1 - \vec{R}_2}{2\xi} & \text{for } j \in \text{DNA}_1 \\ \frac{\vec{R}_2 - \vec{R}_1}{2\xi} & \text{for } j \in \text{DNA}_2 \\ 0 & \text{otherwise} \end{array} \right\}, \tag{4}$$

which is explained in detail in SM Subsection II C. Thus, if we know the total force on the DNA_1 and DNA_2 helices, we can compute the potential of mean force (PMF) as a function of ξ, $\Delta G(\xi)$, by integrating $\langle F_\xi \rangle_\xi$, which is an ensemble average of F_ξ at fixed ξ, over the reaction coordinate ξ:

$$\Delta G(\xi) = -\int \langle F_\xi(\xi) \rangle_\xi d\xi + C, \tag{5}$$

where C is an arbitrary constant. The PMF obtained thereby should be consistent with the PMF computed using the weighted histogram analysis method (WHAM) [8, 11]. Indeed, the forces applied by the harmonic umbrella potentials are in quantitative agreement with the forces computed directly using Eq. (3), Fig. S9 A,B.

In the case of a pairwise force, Eq. (3) can be used to determine the contributions to the PMF from specific types of interactions. Defining the pairwise force from atom k on atom j as $\vec{f}_{jk}$, $\vec{F}_j = \sum_{k=1}^{N} \vec{f}_{jk}$. The contribution of direct DNA-DNA interactions to $F_\xi(\xi)$ can then be computed as

$$F_\xi^{\text{DNA-DNA}}(\xi) = (\sum_{j}^{\text{DNA}_1} \sum_{k}^{\text{DNA}_2} \vec{f}_{jk}) \cdot \frac{\vec{R}_1 - \vec{R}_2}{\xi}. \tag{6}$$

In a similar way, the contribution of an arbitrary group X (e.g., sodium, spermine, chloride, or water) to F_ξ can be computed as

$$F_\xi^{\text{DNA-X}}(\xi) = \sum_{l}^{\text{X}} (\sum_{j=1}^{\text{DNA}_1} \vec{f}_{jl} - \sum_{k}^{\text{DNA}_2} \vec{f}_{kl}) \cdot \frac{\vec{R}_1 - \vec{R}_2}{2\xi}. \tag{7}$$

The contribution of the DNA-X interactions to ΔG is then

$$\Delta G^{\text{DNA-X}}(\xi) = -\int \langle F_\xi(\xi)^{\text{DNA-X}} \rangle_\xi d\xi + C, \tag{8}$$

where C is an arbitrary constant.

To determine the contributions of specific interactions to the PMF obtained from the umbrella sampling simulations, we analyzed the umbrella sampling trajectories recorded in double-precision every 2 ps using a pairwise evaluation scheme for the long-range electrostatic forces. Such a re-evaluation of the long-range electrostatic interactions was essential,

as the original trajectories were obtained using the non-pairwise Ewald summation scheme, which is incompatible with Eq. (3). Specifically, we evaluated the electrostatic forces using the Coulomb formula and a distance cutoff of 16, 32, and 56 Å. To use the 56 Å cutoff, the systems were duplicated in the z-direction frame by frame for each trajectory, ensuring that the cutoff value was shorter than half the system's shortest dimension. Fig. S9 C–E shows the contributions to $\langle F_\xi(\xi)\rangle$ from DNA-DNA, DNA-Na^+, and DNA-Sm^{4+} interactions (both Coulomb and vdW). The cutoff value clearly affects the magnitude of the forces, underestimating the long-ranged electrostatic interactions. To obtain an upper bound estimate for the magnitude of the electrostatic contributions, we replicated each frame of our umbrella-sampling trajectories 10 times along the z direction and computed the Coulombic forces per turn for the resulting systems without a cutoff and periodic boundary condition. Performing such a calculation using the all-atom representation of the system was not feasible because of the large number of required calculations. Instead, we used a custom coarse-grained representation of the system, where only charged moieties were taken into account. Thus, spermine nitrogens, DNA phosphates, sodium, and chloride ions we assigned elementary charge values (e or $-e$), other parts of the systems were neglected. Making such a rather major approximation was justified for this particular calculation as the long-ranged interactions were not expected to depend on the atomic-level detail. Furthermore, electrostatic forces were expected to dominate over vdW interactions for the charged species. The magnitudes of $\langle F_\xi(\xi)\rangle$ obtained using our custom coarse-grained representation were considerably greater than the estimates obtained using the 56 Å cutoff, Fig. S9 C–E. The difference was particularly large for the DNA-Na^+ interactions, as the Na^+ ions were located, on average further from DNA than other species. In contrast, the contribution of water molecules to the interaction free energy computed using the all-atom representation was relatively independent from the cutoff value used for the calculations Fig. S9 F.

C. Derivation of Eq. (4)

Given the reaction coordinate ξ, we assume that we can define a coordinate transformation $\mathcal{F}$ from the Cartesian coordinate $\{x_i, y_i, z_i, \cdots, x_N, y_N, z_N\}$ to generalized coordinates $\{\xi, q_1, \cdots, q_{3N-1}\}$. The generalized coordinates q_i for $i = 1, \cdots, 3N-1$ are arbitrary functions of the Cartesian coordinates. If we assume that the inverse transformation $\mathcal{F}^{-1}$ exists,

Jacobian matrices of the transformation, $J_{\mathcal{F}}$, and the inverse transformation, $J_{\mathcal{F}^{-1}}$, equal

$$J_{\mathcal{F}} = \begin{pmatrix} \partial\xi/\partial x_1 & \partial\xi/\partial y_1 & \cdots & \partial\xi/\partial z_N \\ \partial g_1/\partial x_1 & \partial g_1/\partial y_1 & \cdots & \partial g_1/\partial z_N \\ \vdots & \vdots & \ddots & \vdots \\ \partial g_{3N-1}/\partial x_1 & \partial g_{3N-1}/\partial y_1 & \cdots & \partial g_{3N-1}/\partial z_N \end{pmatrix} \tag{9}$$

and

$$J_{\mathcal{F}^{-1}} = \begin{pmatrix} \partial x_1/\partial\xi & \partial x_1/\partial g_1 & \cdots & \partial x_1/\partial g_{3N-1} \\ \partial y_1/\partial\xi & \partial y_1/\partial g_1 & \cdots & \partial y_1/\partial g_{3N-1} \\ \vdots & \vdots & \ddots & \vdots \\ \partial z_N/\partial\xi & \partial z_N/\partial g_1 & \cdots & \partial z_N/\partial g_{3N-1} \end{pmatrix}. \tag{10}$$

Note that we are interested only in derivatives involving ξ. The partial derivatives of ξ in $J_{\mathcal{F}}$ can be explicitly defined as a function of the Cartesian coordinates:

$$\partial\xi/\partial x_i = \begin{cases} \frac{X_1 - X_2}{\xi}\frac{m_i}{\sum_i m_i} & \text{for } i = 1, \cdots, N_1 \\ \frac{X_2 - X_1}{\xi}\frac{m_i}{\sum_i m_i} & \text{for } i = N_1 + 1, \cdots, N_2 \\ 0 & \text{otherwise} \end{cases}, \tag{11}$$

where X_1 and X_2 are the center of mass coordinates of the DNA molecules projected along the x axis. $\partial\xi/\partial y_i$ and $\partial\xi/\partial z_i$ can be similarly defined. On the contrary, the derivatives of (x_i, y_i, z_i) with respect to ξ in $J_{\mathcal{F}^{-1}}$ cannot be easily computed because the inverse transformation function is undefined. However, under the assumption that transformation $\mathcal{F}$ is invertible, the inverse function theorem says that $J_{\mathcal{F}} \cdot J_{\mathcal{F}^{-1}} = I$ and, therefore,

$$\sum_{i=1}^{N}\{(\partial\xi/\partial x_i)(\partial x_i/\partial\xi) + (\partial\xi/\partial y_i)(\partial y_i/\partial\xi) + (\partial\xi/\partial z_i)(\partial z_i/\partial\xi)\} = 1. \tag{12}$$

One solution that satisfies Eq. (12) is

$$\partial x_i/\partial\xi = \begin{cases} \frac{X_1 - X_2}{2\xi} & \text{for } i = 1, \cdots, N_1 \\ \frac{X_2 - X_1}{2\xi} & \text{for } i = N_1 + 1, \cdots, N_2 \end{cases}, \tag{13}$$

with $\partial y_i/\partial\xi$ and $\partial z_i/\partial\xi$ having similar expressions.

A more formal deviation of Eq. (13) is given by Ruiz-Montero et al. [9, 10] According to Ref. [9], the following relationship holds

$$\frac{\partial}{\partial\xi} = \frac{\nabla\xi \cdot \nabla}{|\nabla\xi|^2} \tag{14}$$

if J is the Jacobian of a globally orthogonal curvilinear set of generalized coordinates. By using Eq. (14), one can obtain a solution equal to Eq. (13).

The validity of Eq. (4) for a system of two particles can be directly verified. For example, lets assume that Cartesian coordinates of two atoms $(x_1, y_1, z_1, x_2, y_2, z_2)$ are transformed to the spherical coordinates:

$$(x_1, y_1, z_1, x_2, y_2, z_2) \mapsto (x_{\rm cm}, y_{\rm cm}, z_{\rm cm}, \xi, \theta, \phi) \tag{15}$$

where

$$4\xi^2 = (x_1 - x_2)^2 + (y_1 - y_2)^2 + (z_1 - z_2)^2 \tag{16}$$

and

$$\left\{ \begin{array}{l} x_1 = x_{\rm cm} + \xi \sin\theta \cos\phi \\ y_1 = y_{\rm cm} + \xi \sin\theta \sin\phi \\ z_1 = z_{\rm cm} + \xi \cos\phi \\ x_2 = x_{\rm cm} - \xi \sin\theta \cos\phi \\ y_2 = y_{\rm cm} - \xi \sin\theta \sin\phi \\ z_2 = z_{\rm cm} - \xi \cos\phi \end{array} \right\}, \tag{17}$$

where $(x_{\rm cm}, y_{\rm cm}, z_{\rm cm})$ is the center of mass of the two atoms. By taking derivatives of Eq. (17) with respect to ξ, one can get the same solution as Eq. (4).

[1] B. Hess, C. Kutzner, D. van der Spoel, and E. Lindahl, J. Chem. Theory Comput. **4**, 435 (2008).

[2] S. Nose and M. L. Klein, Mol. Phys. **50**, 1055 (1983).

[3] W. G. Hoover, Phys. Rev. A **31**, 1695 (1985).

[4] M. Parrinello and A. Rahman, J. Appl. Phys. **52**, 7182 (1981).

[5] T. A. Darden, D. York, and L. Pedersen, J. Chem. Phys. **98**, 10089 (1993).

[6] S. Miyamoto and P. A. Kollman, J. Comput. Chem. **13**, 952 (1992).

[7] B. Hess, H. Bekker, H. J. C. Berendsen, and J. G. E. M. Fraaije, J. Comput. Chem. **18**, 1463 (1997).

[8] E. Darve and A. Pohorille, J. Chem. Phys. **115**, 9169 (2001).

[9] M. J. Ruiz-Montero, D. Frenkel, and J. J. Brey, Mol. Phys. **90**, 925 (1997).

[10] M. Sprik and G. Ciccotti, J. Chem. Phys. **109**, 7737 (1998).

[11] J. Hénin and C. Chipot, J. Chem. Phys. **121**, 2904 (2004).

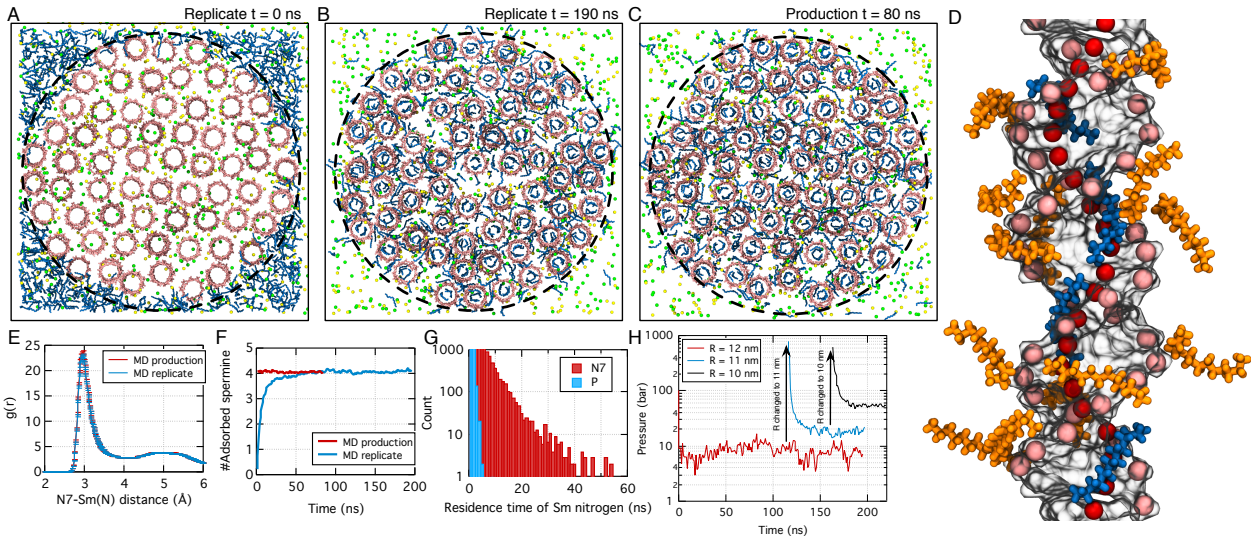

FIG. S1. Replicate simulation of the DNA array system at sub-mM spermine concentration ([Sm^{4+}]). (A) Initial microscopic state used for the replicate simulation. The DNA molecules are shown in pink, Sm^{4+} molecules are shown in blue, Na^+ and Cl^- ions are shown in yellow and green, respectively. For clarity, only DNA backbone is explicitly shown. The dashed line indicates the approximate location of the semi-permeable membrane defining the DNA array of $R = 12$ nm radius. (B, C) Comparison of the final microscopic configurations observed at the end of the replicate (B) and production (C) simulations. (D) A representative conformation of Sm^{4+} molecules near a 20-bp dsDNA molecule (gray transparent surface). Four Sm^{4+} molecules adsorbed to DNA are shown in blue whereas ten Sm^{4+} molecules loosely associated with DNA are shown in orange. The N7 nitrogen and phosphorus (P) atoms of DNA are shown as red and pink spheres, respectively. (E) The radial distribution functions, $g(r)$, of Sm^{4+} nitrogen atoms with respect to the N7 atoms of DNA computed from the replicate (blue) and production (red) simulations. (F) The number of Sm^{4+} molecules adsorbed at a 20-bp dsDNA duplex as a function of the simulation time for the replicate (blue) and production (red) simulations. (G) Residence time of Sm^{4+} nitrogen atoms within the direct contact distance of N7 (red) and P (blue) atoms. The contact distance was determined as the first peak of $g(r)$: 4 and 4.5 Å for N7 and P atoms, respectively. Data in panels E and G were obtained by analyzing the last 80 ns of the respective MD trajectories of the $R = 12$ nm systems. (H) DNA pressure versus simulations time in three replicate simulations carried out at different values of the DNA array radius: $R = 10$ (black), 11 (blue), and 12 (red) nm.

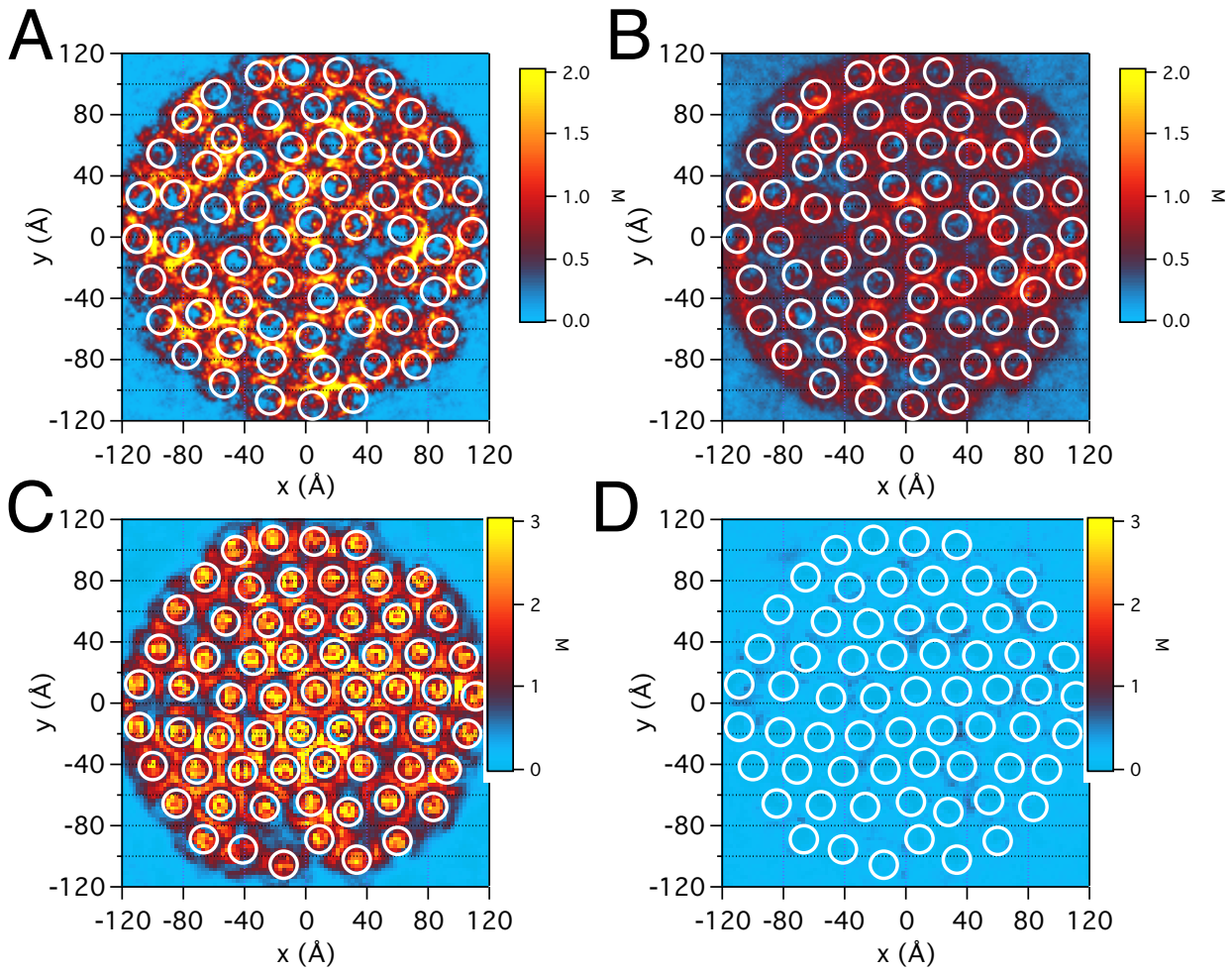

FIG. S2. Distribution of cations in DNA array systems. (A,B) Local distribution of Mg^{2+} (A) and Na^{+} (B) charge and the arrangement of the DNA helices (white circles) in the cross section of a DNA array at $R = 12$ nm and the following bulk electrolyte conditions: $[Mg^{2+}]_b = 20$ mM and $[Na^{+}]_b = 200$ mM. The diameter of each white circle is 2 nm. The data were averaged over the last 20 ns fragment of a ∼100 ns trajectory and over the z axis. (C,D) Local distribution of Sm^{4+} (C) and Na^{+} (D) charge and the arrangement of the DNA helices (white circles) in the cross section of a DNA array at $R = 12$ nm and the following bulk electrolyte conditions: sub-mM $[Sm^{4+}]_b$ and $[Na^{+}]_b = 200$ mM. The diameter of each white circle is 2 nm. The data were averaged over the last 20 ns fragment of a ∼100 ns trajectory and over the z axis.

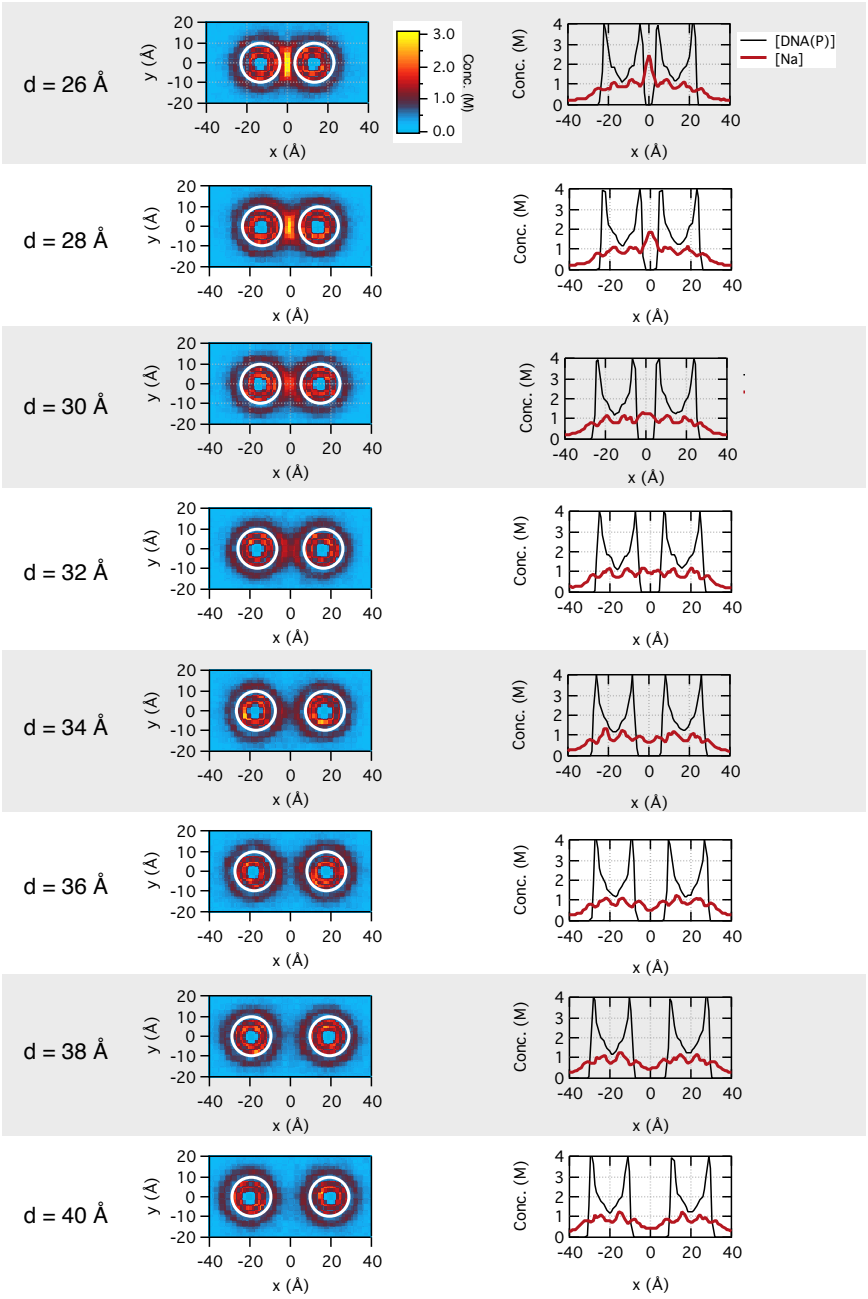

FIG. S3. Ion distribution around a pair of dsDNA molecules at several inter-DNA distances and $[Na^+]_b = 200$ mM. (Left) Local concentration of Na^+ ions around a pair of dsDNA molecules. The heat map shows the concentration of Na^+ ions averaged over the z axis (the directions of the DNA molecules) and the corresponding simulation trajectory. White circles indicate the locations of the DNA helices. (Right) The concentration of DNA phosphorous atoms (black) and Na^+ ions (red) along the x axis computed by averaging the corresponding heat map data over the $y = [-10, 10]$ Å region.

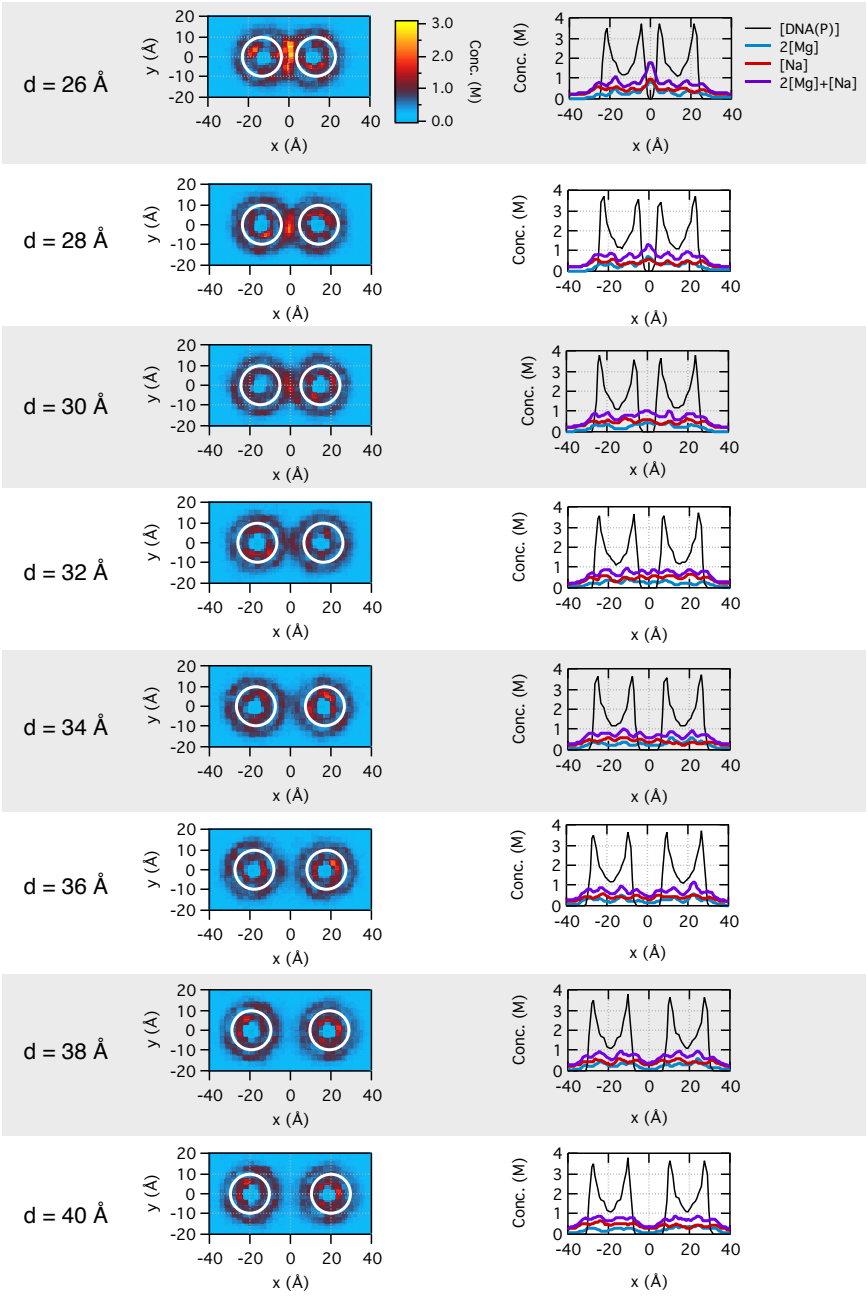

FIG. S4. Ion distribution around a pair of dsDNA molecules at several inter-DNA distances and $[Mg^{2+}]_b = 20$ mM and $[Na^+]_b = 200$ mM. (Left) Local charge density of cations around a pair of dsDNA molecules. The heat map shows the cation charge density, $2[Mg^{2+}]+[Na^+]$, averaged over the z axis (the directions of the DNA molecules) and the corresponding simulation trajectory. White circles indicate the locations of the DNA helices. (Right) The concentration of DNA phosphorous atoms (black), Mg^{2+} (blue) and Na^+ (red) ions along the x axis computed by averaging over the z axis, the corresponding simulation trajectory and the $y = [-10, 10]$ Å region of the corresponding system.

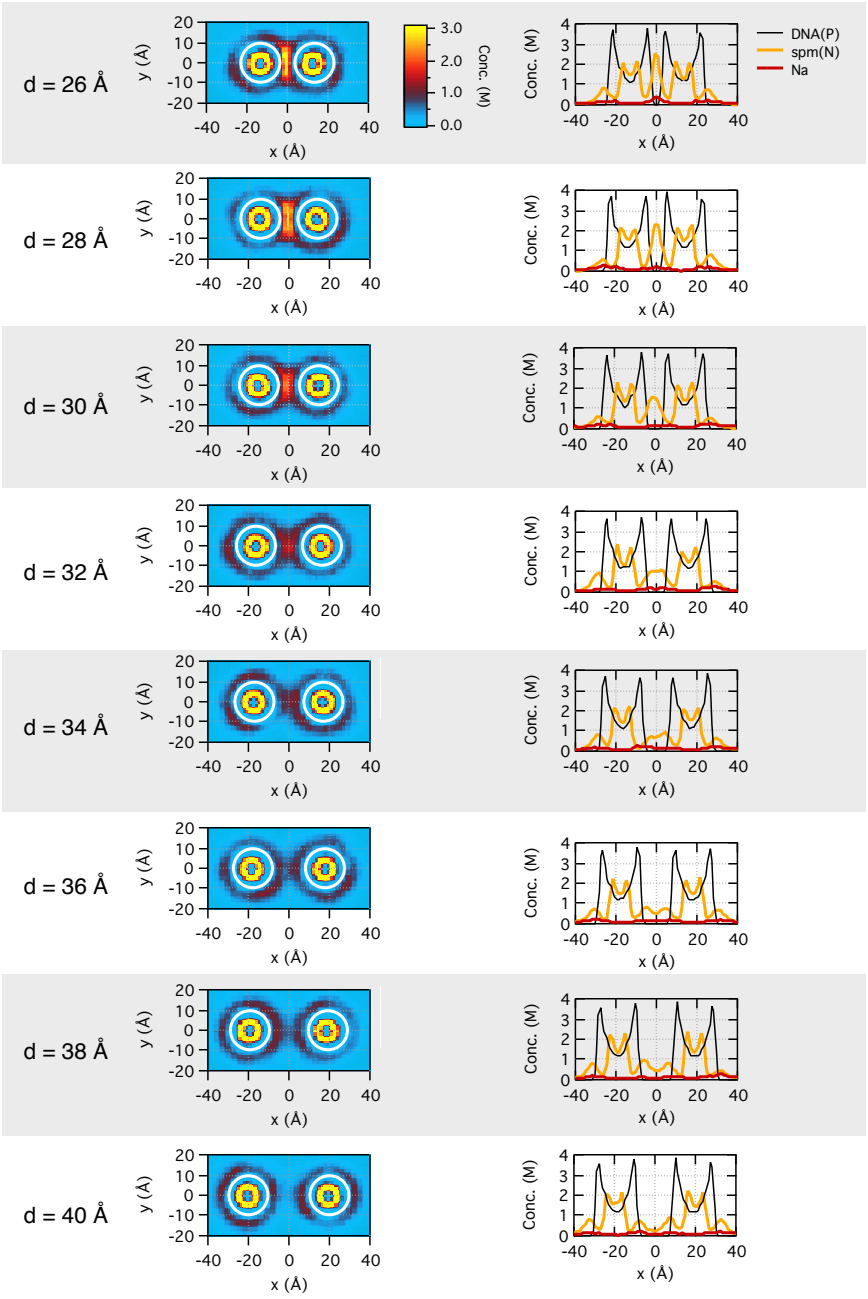

FIG. S5. Ion distribution around a pair of dsDNA molecules at several inter-DNA distances and sub-mM $[Sm^{4+}]_b$ and $[Na^+]_b$ = 200 mM. (Left) Local concentration of Sm^{4+}-amines around a pair of dsDNA molecules. The heat map shows the concentration Sm^{4+}-amines averaged over the z axis (the directions of the DNA molecules) and the corresponding simulation trajectory. White circles indicate the locations of the DNA helices. (Right) The concentration of DNA phosphorous atoms (black), Sm^{4+}-amines (orange) and Na^+ ions (red) along the x axis computed by averaging over the z axis, the corresponding simulation trajectory and the $y = [-10, 10]$ Å region of the corresponding system.

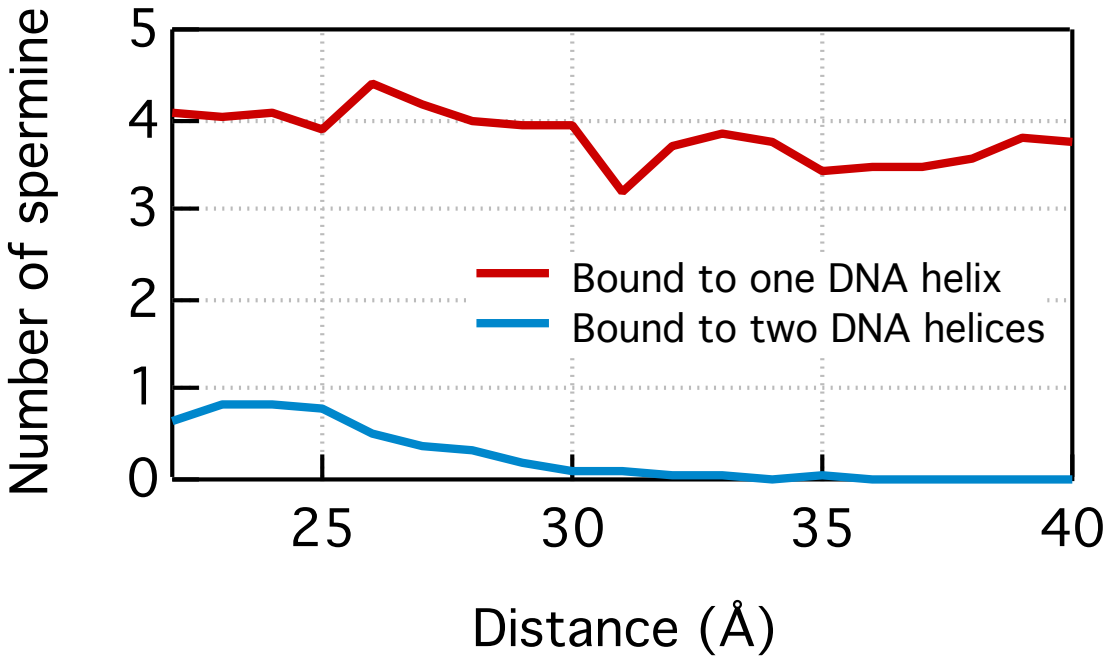

FIG. S6. Direct binding of spermine to DNA. The number of spermine molecules bound directly to one (red) or two (blue) DNA molecules versus the DNA–DNA distance in the simulations of pairwise PMF performed at sub-mM $[Sm^{4+}]_b$ and 200 mM $[Na^+]_b$. In total, twenty Sm^{4+} molecules were present in each simulation system. To count as direct binding, any nitrogen atom of a spermine molecule must be located within 4.5 Å of any phosphorus atom of a DNA helix. Each data point represents a trajectory average.

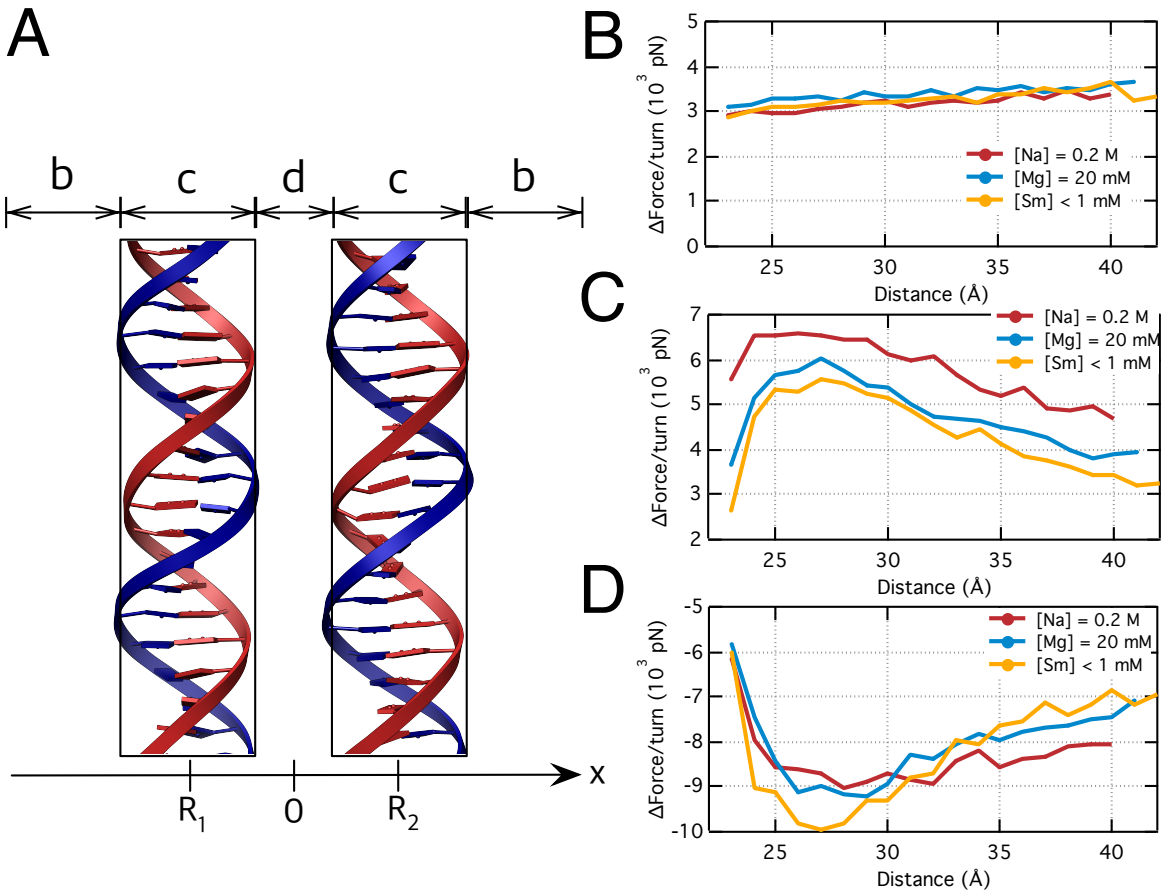

FIG. S7. Decomposition of the Coulomb force according to the spacial location of cations. (A) Definition of the three spacial regions in the system of two DNA molecules: a region away from either helix (region b), $x < (R_1 - 1\text{ nm})$ or $x \geq (R_2 + 1\text{ nm})$; a region surrounding a DNA helix (region c), $(R_1 - 1\text{ nm}) \leq x < (R_1 + 1\text{ nm})$ or $(R_2 - 1\text{ nm}) \leq x < (R_2 + 1\text{ nm})$; and a region between the two helices (region d), $(R_1 + 1\text{ nm}) \leq x < (R_2 - 1\text{ nm})$. In the above expressions, the x coordinate is defined along the line passing through the centers of mass of the two helices, R_1 and R_2, with the origin located exactly between the helices. (B–D) The Coulomb force between DNA and cations located in regions b, c, and d of the two-DNA system, panel A. In each panel, the forces are plotted for the following three systems: $[Na^+]_b = 200$ mM (red), $[Mg^{2+}]_b = 20$ mM and $[Na^+]_b = 200$ mM (blue), and sub-mM $[Sm^{4+}]_b$ and $[Na^+]_b = 200$ mM (orange). The attractive (negative) force is produced by cations located between DNA helices (region d).

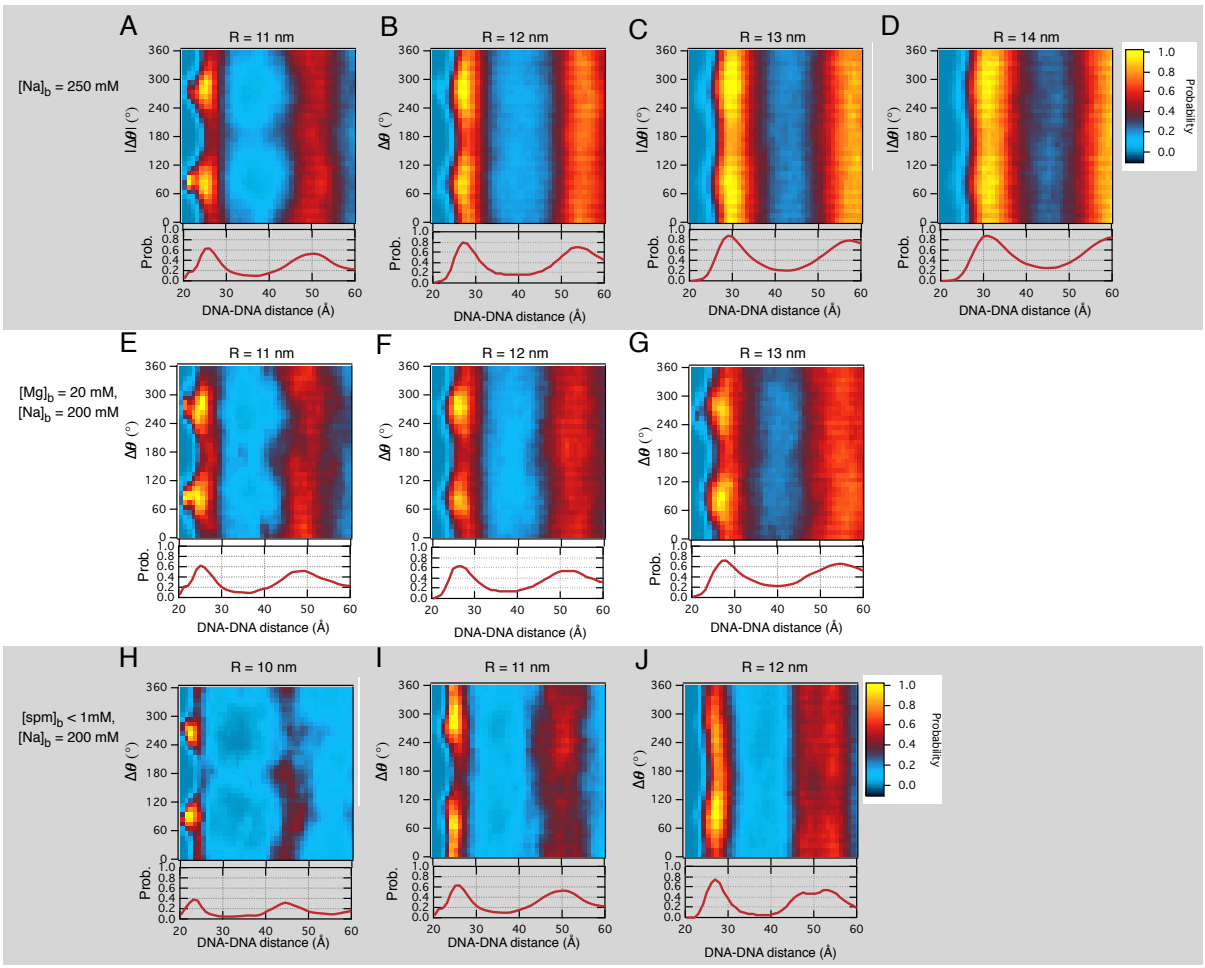

FIG. S8. Relative azimuthal orientation of two neighboring dsDNA molecules in a DNA array simulation. The mutual azimuthal orientation parameter $\Delta\theta$ is defined in Fig. 3A,B of the main text. Each panel shows a 2D density map that characterizes the probability of finding two neighboring DNA molecules of the prescribed DNA–DNA distance and mutual azimuthal orientation. Each panel corresponds to a unique simulation condition.

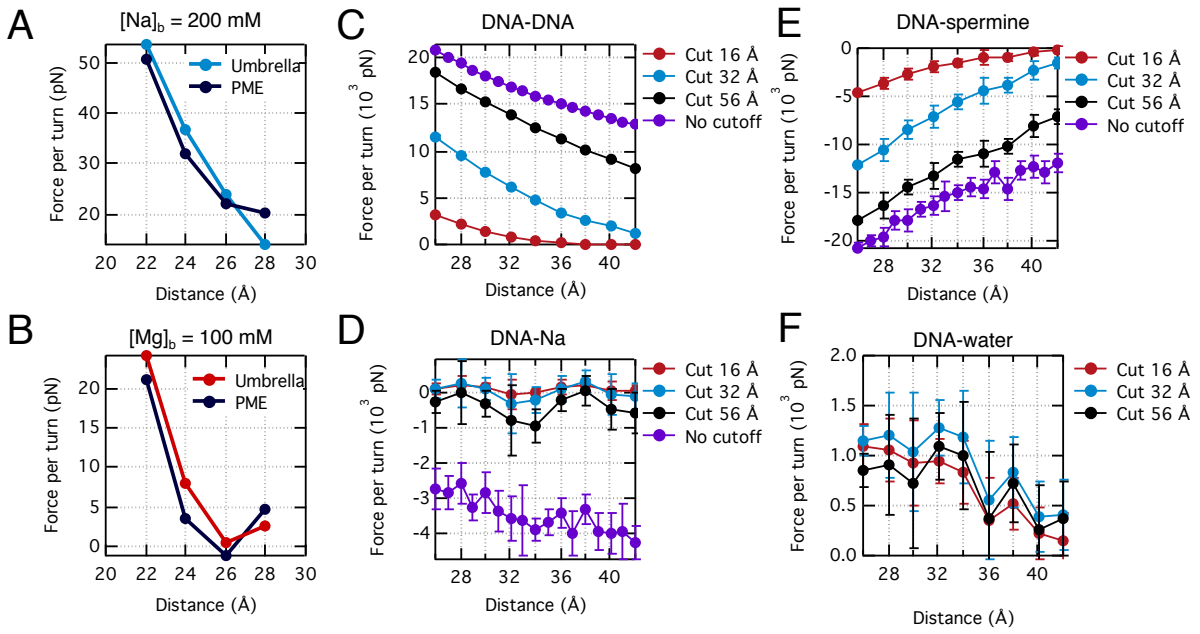

FIG. S9. Calculations of the interaction-type dependent contributions to the PMF. (A,B) The average force between two DNA molecules versus the inter-DNA distance applied by the restraining potentials in the umbrella sampling simulations or computed directly from the atomic coordinates of the system. The direct force calculations reported in these panels employed the PME scheme for evaluation of the long-range electrostatic interactions. The buffer ionic conditions were $[Na^+]_b$ = 200 mM (panel a) and $[Mg^{2+}]_b$ = 100 mM (panel B). In both panels, the inter-DNA force computed directly from the atomic coordinates of the system is in quantitative agreement with the force applied by the restraining potentials, which validates our method for computing the forces directly from the atomic coordinates. (C–E) The direct electrostatic force applied to a DNA molecule in MD simulations of inter-DNA PMF performed at sub-mM $[Sm^{4+}]_b$ and $[Na^+]_b$ = 200 mM. Panels c, d and e specify the direct electrostatic force from the second DNA molecule (C), Na^+ (D) and Sm^{4+} (E) ions for several values of the cutoff distance used for the force evaluation. The original all-atom model was used for the force calculations at distance cutoffs of 16, 32, or 56 Å; a custom coarse-grained representation was used for the force evaluation without a cutoff. (see SM Methods II B). (F) The effects of the distance cutoff on the evaluation of the direct water–DNA force. The forces were evaluated using the all-atom models of the systems and included contributions of both electrostatic and vdW interactions. The results reported in panels f correspond to the PMF simulations at sub-mM $[Sm^{4+}]_b$ and $[Na^+]_b$ = 200 mM.